Production of a large area diffuse arc plasma with multiple cathode*

Cheng Wang(王城)[1,†], Hai-Chao Cui(崔海超)[1], Wan-Wan Li(李皖皖)[1],
Meng-Ran Liao(廖梦然)[1], Wei-Luo Xia(夏维珞)[2], and Wei-Dong Xia(夏维东)[1]

[1] *Department of Thermal Science and Energy Engineering, University of Science and Technology of China, Hefei* 230027, *China*
[2] *Hefei Institutes of Physical Science, Chinese Academy of Sciences, Hefei* 230031, *China*

(Received 9 October 2016; revised manuscript received 3 November 2016; published online 20 December 2016)

An arc channel at atmospheric pressure tends to shrink generally. In this paper, a non-transferred DC arc plasma device with multiple cathode is introduced to produce a large area arc plasma at atmospheric pressure. This device is comprised of a 42-mm diameter tubular chamber, multiple cathode which is radially inserted into the chamber, and a tungsten anode with a nozzle in its center. In argon/helium atmosphere, a large area and circumferential homogenous diffuse arc plasma, which fills the entire cross section surrounded by the cathode tips, is observed. Results show that the uniformity and stability of diffuse arc plasma are strongly related to the plasma forming gas. Based on these experimental results, an explanation to the arc diffusion is suggested. Moreover, the electron excitation temperature and electron density measured in diffuse helium plasma are much lower than those of constricted arc column, which indicates the diffuse helium plasma probably deviates from the local thermodynamic equilibrium state. Unlike the common non-transferred arc plasma devices, this device can provide a condition for axial-fed feedstock particles. The plasma device is attempted to spheroidize alumina powders by using the central axis to send the powder. Results show that the powder produced is usually a typical hollow sphere.

Keywords: multiple cathode, diffuse arc plasma, plasma spheroidization

PACS: 52.75.Hn, 52.70.–m, 52.77.–j **DOI:** 10.1088/1674-1056/26/2/025202

1. Introduction

Arc plasma at atmospheric pressure is widely used in material processing and preparation due to its high temperature, high-energy intensity, high chemical activity, relatively convenient and inexpensive device.[1,2] However, because of the small area, concentrated energy and inhomogeneous parameters of arc plasma, the industrial use of arc plasma encounters several problems, including low yield, low product quality, and poor production efficiency.[3–5] Moreover, the cathode always occupies the position of axial-fed feedstock. The mechanical obstructions may result in the difficulty in axially feeding feedstock particles into the plasma.[6]

To improve the disadvantages of arc plasma, a variety of techniques have been developed in recent years. For instance, expanding plasma is often generated by a cascade arc jet which expands to lower pressure,[7,8] but the method of reducing pressure is not suitable for most of the industry application. Adding materials with low ionization potential such as alkali salts to the arc is used to enhance the electrical conductivity at lower temperatures, which contributes to the expansion of the arc.[9] This method is only partly effective and the adding compounds are often unacceptable. At atmospheric pressure, a large area diffuse arc plasma generated in a magnetically rotating arc is reported.[10–13] Unfortunately, the rotating arc plasma possesses fierce centrifugal flow, which makes it hard to control the technological process in practical applications. Inductively coupled plasma generator could produce large area and lower velocity plasma, and there does not exist the service life nor pollution problem induced by electrode ablation.[14] Nonetheless, such devices suffer low energy efficiency and expensive power supply.

Moreover, a multiple arc system is commonly adopted for providing a large area plasma, such as DC plasma generator with multi-electrode[15,16] and multiphase AC plasma generator with multi-electrode.[17,18] For the former, the large area plasma is obtained actually by the physical addition of several arcs, thus the arc plasma is usually in an unsteady turbulent state. For the latter, the arc is subjected to rapid movement, which because of the persistence of luminosity would give rise to the occurrence of a diffuse discharge, so the arc plasma is still discrete and unstable. Despite the problems mentioned, this kind of device has been widely applied, since it can offer a large area plasma and an appropriate space for axial-fed feedstock particles.

To produce a large area and stable diffuse arc plasma, a non-transferred DC plasma device with multiple cathode is built in this study. The arc discharge in the chamber is observed by a high-speed CCD camera. The optical emission spectrum is employed to diagnose the electron excitation temperature and electron density of arc plasma. Through analyzing the effects of plasma forming gas on the arc plasma profile, the formation mechanism and stable conditions for diffuse arc

*Project supported by the National Natural Science Foundation of China (Grant Nos. 11475174 and11035005) and the Fundamental Research Funds for the Central Universities, China (Grant No. WK2090130021).

†Corresponding author. E-mail: awcheng@mail.ustc.edu.cn

© 2017 Chinese Physical Society and IOP Publishing Ltd

plasma are discussed. Moreover, applications of the device to spheroidizing alumina powders are tested by using the central axis to send the powder.

2. Experimental apparatus

Figure 1 shows a longitudinal section view of DC arc plasma device and its experimental setup. The arc chamber is composed of a 42-mm inner diameter cylinder. One of the chamber ends is covered by an anode. The anode is comprised of a 40-mm thick block tungsten with a 10-mm diameter nozzle (40-mm length) in its center. Six cathodes constituting the multiple tungsten cathode, each with 2-wt% lanthana, 5-mm diameter, 40-mm length, and 60° cone angle of the top, are radially inserted into the chamber. The cathode tips are distributed at vertexes of a concentric polygon (the diagonal distance between cathode tips is 20 mm–40 mm). The vertical distance from the cathode tip to the anode is about 15 mm. Through the gap of the chamber wall where the cathodes are inserted, plasma-forming gas is introduced. Another end of the arc chamber is covered with a glass window, around which a window protection gas is introduced through the inlet radially. The volume flow ratio of protection gas to plasma-forming gas is 1:1. Six modulated 0 V–200 V and 0 A–180 A DC power supplies with a common anode are applied to the device and each cathode is connected to a power supply independently. A high-speed CCD camera (Photron company, FASTCAM SA5 1000K-M3) is employed to observe the arc discharge in the chamber. The recording frame rate is 10^3–10^5 frames/s and the exposure time is 0.5 μs–100 μs. Each frame consists of 256×256 pixels with 256 gray levels. The inner surfaces of anode and chamber are painted black to reduce reflections. We image the plasma arc onto a screen via a lens, and map spectral irradiance through the screen with a hole that precisely adjusts the fiber probe of the spectrometer (Princeton Instruments, Acton, SP-2758). A translation stage is employed to adjust the fiber probe position accurately. In the following sections, the diagonal distance between cathode tips is about 30 mm, and the arc currents mean the total currents through all cathodes.

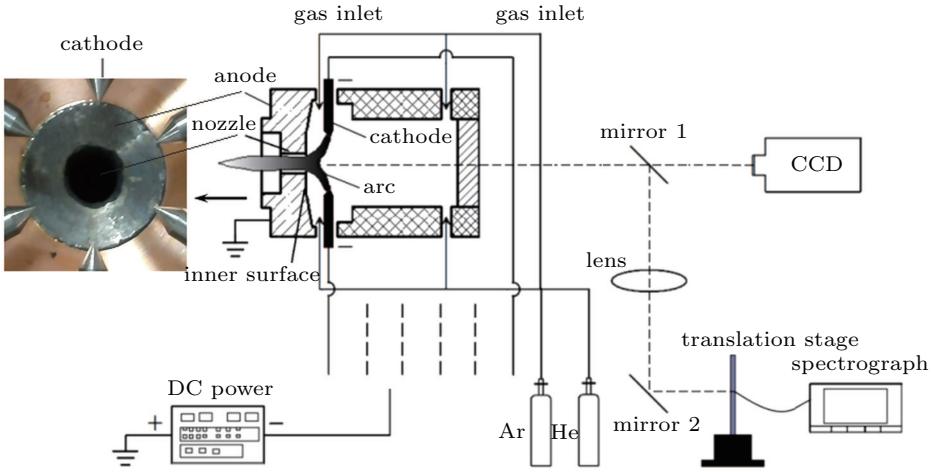


Fig. 1. (color online) Schematic diagram of the arc plasma device and experimental setup.

3. Results and discussion

3.1. Discharge characteristics

A typical window-viewed image of helium arc discharge in the chamber is exhibited in Fig. 2. As noted earlier, six independent DC power supplies are connected to each cathode, however, there are not six discrete discharge channels nor six discrete anode arc roots in the experimental range (200 A–400 A arc currents). In the area of the anode nozzle, there exists a luminous arc column which results from the aggregation of arc plasma. The cathode arc root shown in Fig. 2 is operated in the diffuse mode, thus no luminous spots can be observed in the cathode tips. Between the anode nozzle and cathode tips, the arc plasma presents a relatively uniform and low-density state. The arc appearance is similar to the diffuse arc under an axial magnetic field, so we call it "diffuse arc".

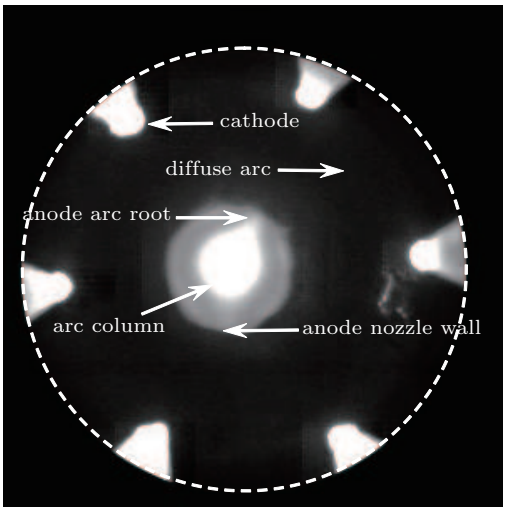


Fig. 2. Window viewed image of arc discharge. I = 240 A, total 1.0 N·m^3/h, helium gas, 1-μs shutter, 5000 frames/s.

Figures 3 and 4 show the successive images of arc plasma and arc voltage curves under different plasma-forming gases. Figure 5 reveals the radiation intensity distributions along the circles (Φ20 mm) and radiation intensity at a fixed point within 10 ms. In the pure argon gas, the cathode arc roots are extremely constricted, showing luminous spots around the cathode tips. Under the effects of electromagnetic forces of cathodes and arcs, the cathode arc roots are often located on one side of each of the cathodes instead of on the cathode tips. The arc plasma between cathode tips and anode nozzle is diffuse, but the radiation intensity distributions in time and space shown in Fig. 5 indicate that the diffuse arc is neither homogenous nor stable. Accordingly, the arc voltage fluctuation is more than 11 V (30% fluctuation) as shown in Fig. 4. Frames 1–4 in Fig. 3 reveal that several luminous spots appear in the diffuse arc, and these spots develop downstream gradually. This phenomenon can be explained as the fact that the breakdown between the arc and anode inner surface occurs, thus the uniformity and stability of diffuse arc are severely affected.

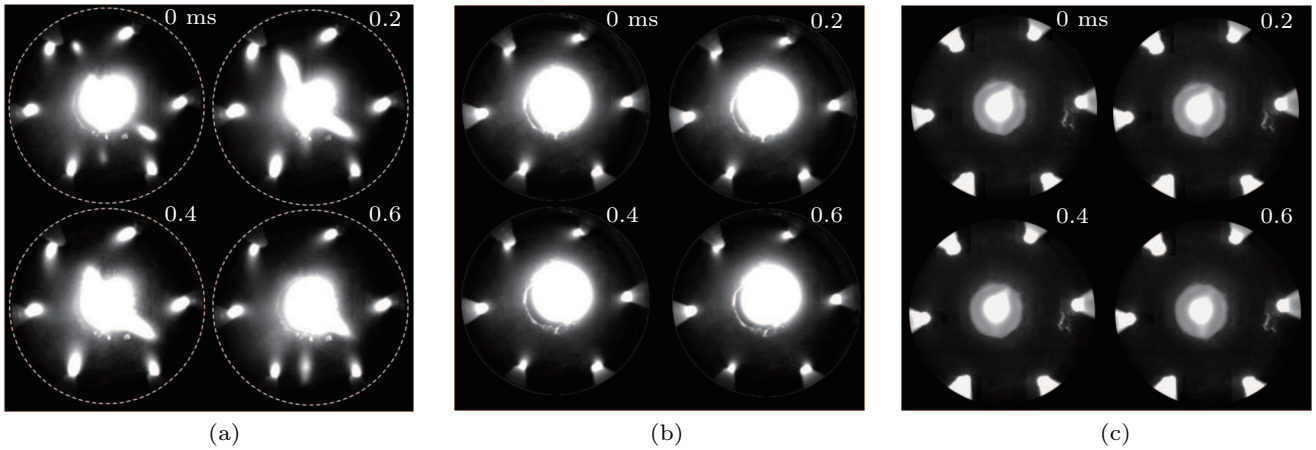


Fig. 3. Successive images of arc plasma under different plasma-forming gases. $I = 240$ A, total 1.0 N·m^3/h, 1-μs shutter, 5000 frames/s, in (a) pure Ar, (b) mixture of Ar and He with a volume flow rate: Ar:He = 1:1, and (c) pure He.

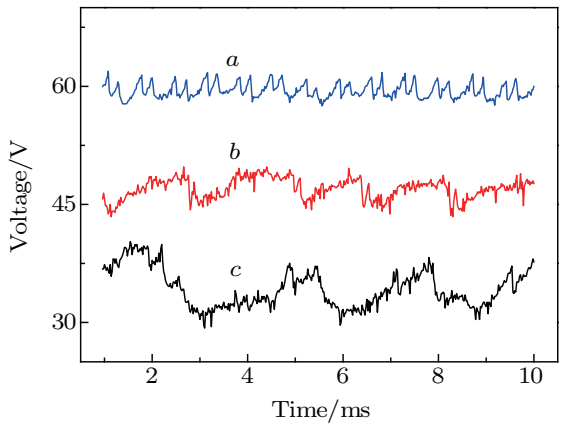


Fig. 4. (color online) Arc voltage waves corresponding to the discharges in Fig. 3.

As the helium gas rate increases to 50%, the diffuse arc plasma becomes much more uniform and stable than pure argon gas as exhibited in Figs. 3–5. The arc voltage increases sharply because the helium has lower electrical conductivity, but the voltage fluctuation is less than 7 V (15% fluctuation). The area of each luminous cathode spot is reduced and no obvious breakdown phenomena appear in the diffuse arc. Nevertheless, the radiation intensity distribution in Fig. 5 indicates that the fluctuation is more than 50%, thus the diffuse arc is not stable enough. A large number of CCD images show that the arc column moves around the anode nozzle entrance slightly, that may be the main factor to cause the instability.

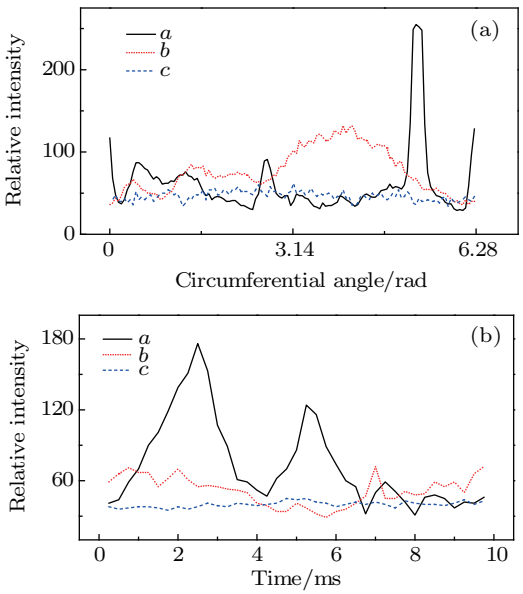


Fig. 5. (color online) (a) Radiation intensity distributions along the circles (Φ20 mm) and (b) radiation intensities at a fixed point (0π) within 10 ms.

When the pure helium gas is used, the arc voltage increases to 60 V, but the voltage fluctuation decreases to 8% (less than 5-V fluctuation). Figure 3 shows the cathode arc root cannot be observed, which indicates the constricted root has already been transformed into a diffuse one. The area of the luminous spot in the anode nozzle is further reduced, meanwhile, we hardly find any breakdown phenomena in the

diffuse arc. Therefore, the diffuse helium arc presents an excellent stability and uniformity (less than 10% fluctuation in terms of time and space) as shown in Figs. 3–5.

In contrast with the diffuse arc in rotating arc generator, the arc diffusion in this paper is a spontaneous process without any rigorous conditions such as external magnetic field, complicated flow field, etc.[12,19] The formation of diffuse arc in this paper is not clear now, herein, we infer that the arc diffusion is mainly attributed to the specific arrangement of cathodes. Due to the existence of self-induced magnetic field, the adjacent arcs always attract each other under the action of Lorentz force, so the arcs have circumferential development trends. Moreover, the cathodes of ring-shaped arrangement increase the boundary temperature, which also benefits arc expansion. The diffuse cathode arc root is a necessary condition for the uniformity of diffuse arc.[19,20] In practice, because of fabrication error, asymmetric cathode structure, small disturbance, etc, the constricted cathode arc root can be very easily deviated from the cathode tip and this can lead to asymmetry existing in the diffuse arc. When the constricted root becomes a diffuse one, the asymmetry of the arc root can be ignored. This is one of the important reasons why the diffuse helium arc is much more uniform than the argon arc. Most of the phenomena observed so far indicate the instability of the diffuse arc mainly comes from the breakdown between arc plasma and anode inner surface. The breakdown occurrence is mainly determined by two factors. One is the thickness of the cold-gas boundary layer between the anode inner surface and the arc, and the other is the cold-gas type. The previous research[21] shows that, because the helium has lower electrical conductivity, the high-temperature region of the arc decreases gradually with the increase of helium content. Thus, the volume of helium arc is smaller than that of the argon arc under the same arc currents, so that the thickness of the cold-gas boundary layer is larger accordingly. In addition, the breakdown voltage of the helium is also much higher than that of argon. Hence, using some plasma-forming gases of lower electrical conductivity is not conducive to the breakdown occurrence, thereby improving the arc stability.

Figure 6 shows the plasma jet appearances under different plasma-forming gases. In pure argon gas, the jet length is less than 7 cm and high noise occurs. The flow can be considered to be in a turbulent state. With the increase of helium content, the plasma jet length increases and the noise decreases gradually, which indicates that the plasma jet is transformed from the turbulent state to the laminar one. When pure helium gas is imposed, the plasma jet has a laminar-like appearance, keeping their stable length and silent flow state. The maximum length of the jet is more than 50 cm and the ratio of the length to the nozzle diameter exceeds 50. The variation of plasma gas composition can change plasma parameters, such as plasma power, plasma velocity, etc., which may change the plasma jet appearance. Besides, the stability of the arc is also a key factor that affects the plasma jet appearance. In this experiment, the trend of jet variation is in accord with that of the diffuse arc stability. Thus, we suggest that the stable diffuse arc may be beneficial to the generation of a long and stable plasma jet.

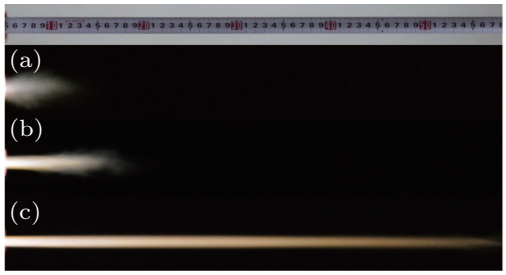


Fig. 6. (color online) Plasma jet appearances corresponding to those in Fig. 3.

3.2. Excitation temperature and electron density

The excitation temperature $(T_{\rm exc})$ of a diffuse arc is determined by the Boltzmann plot method from the following equation:

$$\ln\left(\frac{I_{nm}\lambda_{nm}}{g_nA_{nm}}\right) = -\frac{1}{k_{\rm B}T_{\rm exc}}E_n + C,$$

where I_{nm} is the radiation intensity, λ_{nm} is the wavelength, A_{nm} is the transition probability, E_n is the excitation energy, g_n is the statistical weight of the upper state, $k_{\rm B}$ is the Boltzmann constant, and C is a constant. By plotting $\ln\left(I_{nm}\lambda_{nm}/g_nA_{nm}\right)$ versus E_n, we obtain the excitation temperature from the slope of the Boltzmann fitted straight line. Seven well-isolated He I lines 388.865 nm, 447.148 nm, 471.314 nm, 501.568 nm, 587.562 nm, 667.815 nm, and 706.519 nm are used in this study. However, the plasma emission collected results from the integration of spectral intensity along the line of sight. The calculated temperature is referred to average temperature.[22] A typical spectra and Boltzmann plots of the seven helium atomic lines are illustrated in Figs. 7 and 8 respectively. The excitation temperature calculated in Fig. 8 is 10385 K.

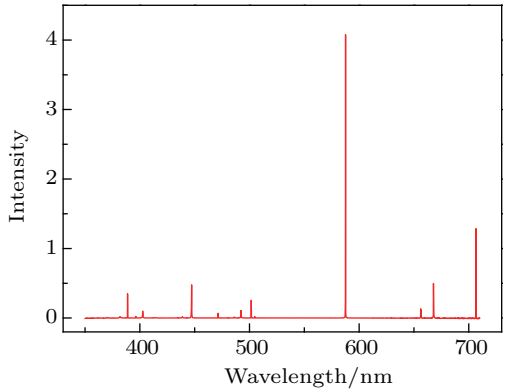


Fig. 7. (color online) Measurement of spectral radiance of the diffuse arc at $R = 9$ mm.

The electron density of the diffuse arc is calculated from the Stark broadening of the helium atomic lines. For the 667.815-nm He I line, the fit, which has been done in a range of electron density close to 10^{16} cm^{-3}, gives the following result:[23–25]

$$\ln\omega(\text{Å}) = -34.90(\pm1.5) + 1.040(\pm0.014)\ln N_e(\text{cm}^{-3}) - 0.35(\pm0.04)\ln T_e(\text{K}),$$

where ω is the Stark broadening, N_e is the electron density, and T_e is the electron temperature.

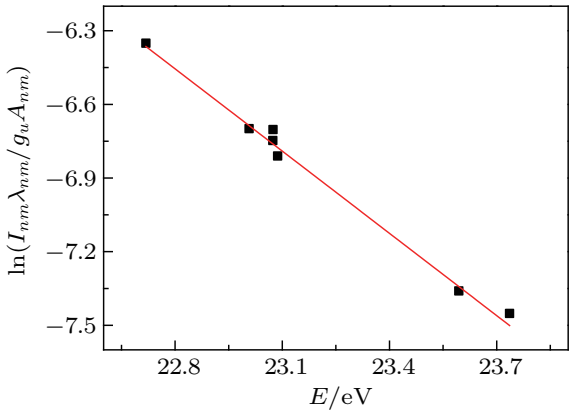


Fig. 8. (color online) Typical Boltzmann plot for the selected He I lines obtained inside the diffuse arc at $R = 9$ mm.

In our experiment, the total width of the spectral line is a convolution of the Lorentzian profile (ω_L, Stark broadening) and the Gaussian profile (ω_S, Doppler broadening and instrumental broadening). The Stark broadening of the recorded spectral line is obtained by fitting a Voigt function. Figure 9 displays a typical recorded He I 667.8-nm line profile with a calculated Voigt function.

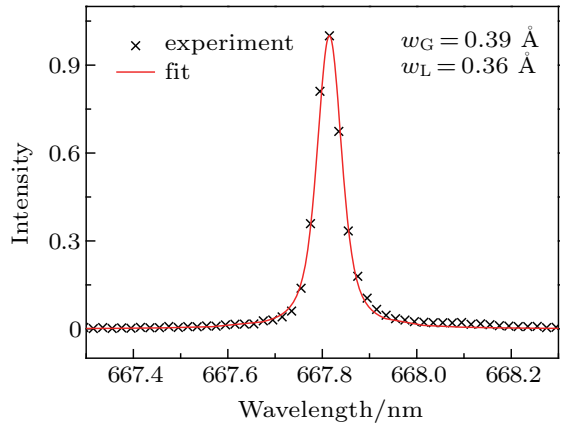


Fig. 9. (color online) Typical Voigt fit of the recorded He I 667.815-nm line obtained inside the diffuse arc at $R = 5$ mm.

Figure 10 represents the radial distributions of excitation temperature and electron density in diffuse helium arc. It shows that both the excitation temperature and electron density exhibit a falling evolution in the radial direction, decreasing from 11890 K and $3.15.\times10^{15}$ cm^{-3} at $R = 5$ mm near the anode nozzle to 6444 K and $1.18.\times10^{15}$ cm^{-3} at $R = 15$ mm between two cathode tips.

Excitation temperatures are expected to be close to the electronic ones. But the experimental measurement values are much lower than the electronic temperatures in constricted helium arc under 30 A–300 A arc currents (above 13000 K).[26] The electron density is also lower than that in a constricted helium arc, and it is of the order of 10^{16} cm^{-3}. Hence, the results indirectly demonstrate that the arc column is diffuse rather than constricted. Kolesnikov[27] reported that the electron density is often more than 10^{16} cm^{-3} when the helium arc is close to the local thermodynamic equilibrium (LTE) state at atmospheric pressure. The experimental result suggests that the diffuse helium arc plasma probably deviates from the LTE state.

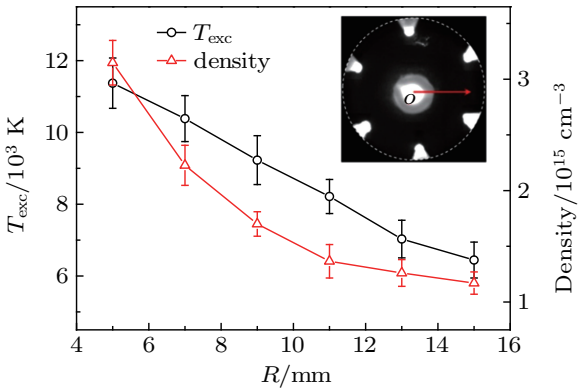


Fig. 10. (color online) Distributions of excitation temperature and electron density in the radial direction. $I = 240$ A, total 1.0 N·m^3/h.

3.3. Applications for spheroidizing alumina powders

Compared with the traditional plasma torches, this device with ring-shaped arrangement of multiple cathodes offers an appropriate space for axially-fed feedstock particles. On the other hand, the large area diffuse plasma and stable laminar jet may provide a more uniform technological condition for material processing. In this paper, the device is used for spheroidizing alumina powders. The size of alumina powders is 600 mesh, and impurity levels of the powders in terms of total content are below 0.5%. We adopt the method of using the central axis to send the powder. The powders are fed through an injection probe to the arc plasma flame by proper carrier gas. The inner diameter of injection probe is 3 mm, and the probe outlet is located 5 mm above the plane of cathode tips. The carrier gas is argon gas and the plasma-forming gas is helium gas, and their flow rates are 0.3 N·m^3/h and 1 N·m^3/h respectively. The powder feed rate is about 20 g/min. The particles after plasma process are directly injected into a distilled water container for cooling and collecting. The arc power is about 10 kW (240 A, 42 V). The microstructural (SEM) images of particles are performed on a Sirion 200 apparatus.

Figure 11 gives the SEM images of alumina feedstock particles and produced particles. Comparison between

Figs. 11(a) and Fig. 11(b) shows that the spheroidization takes place effectively. The surfaces of produced particles are rough and covered with a few nano-sized particles which come from the partial or complete evaporations of alumina powders. The formation mechanism of spherical particles can be explained as the fact that in the high temperature condition of thermal plasma, the feedstock particles with irregular shapes melt rapidly. When the particles leave the plasma flame, the molten droplets cool quickly and solidify into relatively uniform spheres ultimately.

Figure 12 reveals the interiors of the produced particles cut by a diamond blade. Our results indicate that the alumina particles after spheroidization are typically hollow spheres. The walls of the individual particles may differ by a considerable extent as this can be recognized by comparing Fig. 12(a) with Fig. 12(b). The difference can be ascribed to the fact that the alumina particles may have different motion trajectories in the arc plasma. It is noteworthy that there are even several small pores within each particles produced as shown in Fig. 12(b).

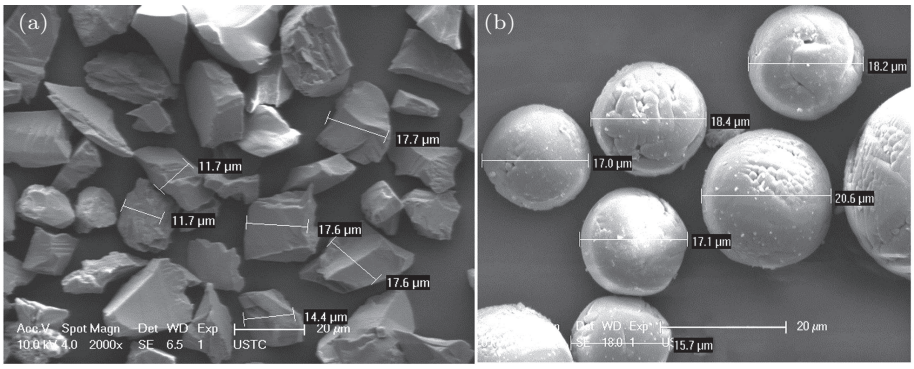


Fig. 11. SEM images of (a) alumina feedstock particles and (b) alumina particles after spheroidization.

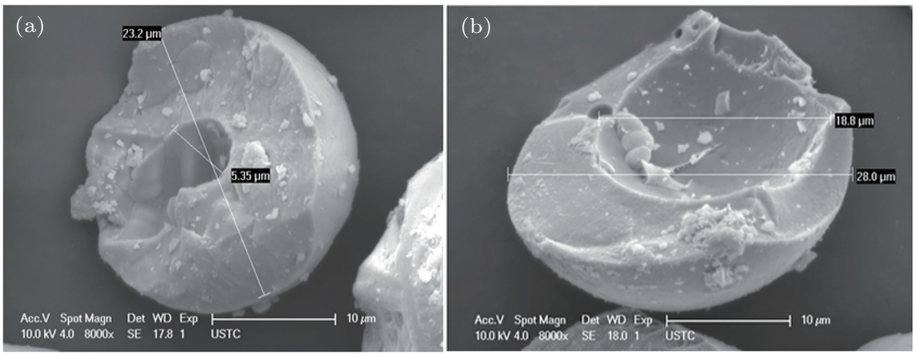


Fig. 12. SEM images of the particles produced cut by a diamond blade, showing (a) a single pore, (b) a big pore with several small pores.

Production of hollow ceramic microspheres has received more and more attention due to their excellent performances including lower density, lower permittivity, higher specific surface area, and higher thermal strain tolerance.[28–30] In general, a porous structure of raw material is considered to be indispensable for creating the hollows. The raw material is often constituted by primary particles of several microns by spray drying or agglomeration.[31–33] In this study, the device may provide a convenient way of obtaining hollow spherical particles because the pretreatment of raw material is not necessary any more. It is noticed that hollow particles may result from the densities of the particle material in the solid and liquid state, and the overheating value of the droplets.[34] The diffuse arc plasma and long laminar plasma jet might provide a proper heating condition which is favorable for the occurrence of the above-mentioned process. The influence mechanism is not well understood, nevertheless, this device supplies a suitable method of directly forming the hollow particles.

4. Conclusions

In this paper, a non-transferred DC arc plasma device with multiple cathode is designed to produce a large area arc plasma at atmospheric pressure. The diffuse arc plasma which almost fills the entire circular cross section surrounded by the cathode tips is achieved. The characteristics of diffuse arc, including arc appearance, arc uniformity and stability are investigated experimentally. The optical emission spectrum is employed to diagnose the electron excitation temperature and electron density of arc plasma. Besides, the use of the device for spheroidizing alumina powders is tested. The main conclusions gained are as follows.

(i) The diffuse plasma presents better uniformity and sta-

bility with the increase of helium content. The formation of a diffuse arc may be mainly attributed to the self-induced magnetic field of adjacent arcs, and the uniformity and stability of the diffuse arc are dependent on the cathode arc modes and gas electrical conductivity.

(ii) The electron excitation temperature and electron density of the diffuse helium plasma are much lower than those in the constricted arc column under the same current. This phenomenon indicates that the diffuse arc probably deviates from the LTE state.

(iii) Contrary to the common plasma torches, this device can provide a proper condition for axial-fed feedstock particles. Plasma spheroidization of alumina powders indicates that the spherical particles produced have a hollow structure each. This device is expected to possess promising application in material processing, fine particles' preparation, plasma spraying, etc.

References

[1] Fauchais P and Vardelle M 1994 *Pure Appl. Chem.* **66** 1247
[2] Schutze A, Jeong J Y, Babayan S E, Park J, Selwyn G S and Hicks R F 1998 *Ieee Trans. Plasma Sci.* **26** 1685
[3] Schmidt C E and Sacks R D 1983 *Spectrochimica Acta Part B-Atomic Spectroscopy* **38** 557
[4] Fauchais P and Vardelle A 1997 *IEEE Trans. Plasma Sci.* **25** 1258
[5] Pfender E 1999 *Plasma Chemistry and Plasma Processing* **19** 1
[6] Herman H, Sampath S and McCune R 2000 *Mrs Bulletin* **25** 17
[7] Buuron A J M, Vandesanden M C M, Vanooij W J, Driessens R M A and Schram D C 1995 *J. Appl. Phys.* **78** 528
[8] Schram D, Mazouffre S, Engeln R and van de Sanden M 2001 "The physics of plasma expansion", in *Atomic and Molecular Beams* (Berlin: Springer) p. 209
[9] Lawton J 1975 *Physics in Technology* **6** 190
[10] Slinkman D and Sacks R 1990 *Appl. Spectros.* **44** 76
[11] Slinkman D and Sacks R 1990 *Appl. Spectros.* **44** 83
[12] Xia W D, Li L C, Zhao Y H, Ma Q, Du B H, Chen Q and Cheng L 2006 *Appl. Phys. Lett.* **88** 211501
[13] Wang C, Li W W, Zhang X N, Liao M R, Zha J and Xia W D 2015 *IEEE Trans. Plasma Sci.* **43** 3716
[14] Kawajiri K, Sato T and Nishiyama H 2003 *Surf. Coat. Technol.* **171** 134
[15] Vijvers W A J, de Groot B, Al R S, van den Berg M A, van Eck H J N, Goedheer W J, Kleyn A W, Koppers W R, Kruijt O G, Cardozo N J L, van der Meiden H J, van de Pol M J, Prins P R, Rapp J, Schram D C, Shumack A E, Smeets P H M, Westerhout J, Wright G M and van Rooij G J 2009 *Fusion Eng. Design* **84** 1933
[16] Ageorges H, Megy S, Chang K, Baronnet J M, Williams J K and Chapman C 1993 *Plasma Chemistry & Plasma Processing* **13** 613
[17] Harry J E and Knight R 1981 *IEEE Trans. Plasma Sci.* **9** 248
[18] Yao Y C, Watanabe T, Yano T, Iseda T, Sakamoto O, Iwamoto M and Inoue S 2008 *Sci. Technol. Adv. Mater.* **9** 25013
[19] Wang C, Li W W, Zhang X N, Zha J and Xia W D 2015 *Chin. Phys. B* **24** 065206
[20] Xia W D, Zhou H L, Zhou Z P and Bai B 2008 *IEEE Trans. Plasma Sci.* **36** 1048
[21] Chenming X, Hongming G, Guangjun Z and Lin W 2005 *Vacuum* **77** 111
[22] Tu X, Cheron B G, Yan J H, Yu L and Cen K F 2008 *Phys. Plasmas* **15** 053504
[23] Perez C, Delarosa I, Defrutos A M and Mar S 1991 *Phys. Rev. A* **44** 6785
[24] Perez C, delaRosa I, Aparicio J A, Mar S and Gigosos M A 1996 *Jpn. J. Appl. Phys.* **35** 4073
[25] Bardet J P, Valognes J C and Vitel Y 2000 *J. Quantum Spectros. Rad. Transfer* **65** 853
[26] Terasaki H, Tanaka M and Ushio M 2002 *Metallurgical and Materials Transactions a-Physical Metallurgy and Materials Science* **33** 1183
[27] Kolesnikov V 1964 *Tr. Inst. Fiz. Akad. Nauk SSSR Ira. P. N. Lebedev* **30** 66
[28] Gulyaev I P and Solonenko O P 2013 *Experiments in Fluids* **54**
[29] Zhang X F, Zhou K S, Chen H T, Han T, Song J B and Liu M 2015 *Rare Metal Mater. Eng.* **44** 1301
[30] Solonenko O P, Nishiyama H, Smirnov A V, Takana H and Jang J 2015 *J. Visualization* **18** 1
[31] Karoly Z and Szepvolgyi J 2005 *Chemical Engineering and Processing* **44** 221
[32] Karoly Z and Szepvogyi J 2003 *Powder Technology* **132** 211
[33] Pravdic G and Gani M S J 1996 *J. Mater. Sci.* **31** 3487
[34] Solonenko O P, Gulyaev I P and Smirnov A V 2011 *J. Therm. Sci. Technol.* **6** 219